

No-Box Attacks on 3D Point Cloud Classification

Hanieh Naderi, *Student Member, IEEE*, Chinthaka Dinesh, *Member, IEEE*, Ivan V. Bajić, *Senior Member, IEEE*, and Shohreh Kasaei, *Senior Member, IEEE*

Abstract—Adversarial attacks pose serious challenges for deep neural network (DNN)-based analysis of various input signals. In the case of 3D point clouds, methods have been developed to identify points that play a key role in network decision, and these become crucial in generating existing adversarial attacks. For example, a saliency map approach is a popular method for identifying adversarial drop points, whose removal would significantly impact the network decision. Generally, methods for identifying adversarial points rely on the access to the DNN model itself to determine which points are critically important for the model’s decision. This paper aims to provide a novel viewpoint on this problem, where adversarial points can be predicted without access to the target DNN model, which is referred to as a “no-box” attack. To this end, we define 14 point cloud features and use multiple linear regression to examine whether these features can be used for adversarial point prediction, and which combination of features is best suited for this purpose. Experiments show that a suitable combination of features is able to predict adversarial points of four different networks – PointNet, PointNet++, DGCNN, and PointConv – significantly better than a random guess and comparable to white-box attacks. Additionally, we show that no-box attack is transferable to unseen models. The results also provide further insight into DNNs for point cloud classification, by showing which features play key roles in their decision-making process.

Index Terms—Point cloud processing, adversarial example, no-box attack, graph signal processing, multiple linear regression.

I. INTRODUCTION

Deep Neural Networks (DNNs) have become a go-to approach for many problems in image processing and computer vision [1]–[4] due to their ability to model complex input-output relationships from a relatively limited set of data. However, studies have also shown that DNNs are vulnerable to adversarial attacks [5], [6]. An adversarial attack involves constructing an input to the model (adversarial example) whose purpose is to cause the model to make a wrong decision. Much literature has been devoted to the construction of 2D adversarial examples for image analysis models and the exploration of related defenses [5]–[9]. Research on adversarial attacks and defenses has gradually expanded to 3D point cloud models as well, especially point cloud classification [10]–[14].

Point clouds themselves have become an increasingly important research topic [15]–[18]. Given a deep model for

point cloud classification, a number of methods have been proposed to determine critical points that could be used in an adversarial attack [19]–[21]. For example, Zheng *et al.* [19] proposed a differentiable method of shifting points to the center of the cloud, known as a *saliency map technique*, which approximates point dropping and assigns contribution scores to input points based on the resulting loss value. Other methods to determine critical points similarly try to estimate the effect of point disturbance on the output.

Once the critical points have been determined, they can be used to create adversarial examples. Several recent studies [10], [11], [22] use critical points as initial positions and then introduce perturbations to create attacks. Usually, some distance-related criteria, such as Hausdorff [11] or the Chamfer distance [11], are used to constrain perturbations around critical positions. Instead of perturbation, another kind of attack drops the critical points; for example, the well-known Drop100 and Drop200 attacks [19] drop, respectively, 100 and 200 points from the point cloud in order to force the model to make a wrong decision. These are considered to be among the most challenging attacks to defend against [10], [23]–[25].

The methods mentioned above, and others in the literature, require access to the DNN model in order to determine critical points. For example, “white-box” attacks have access to the model’s internal architecture and parameters, while “black-box” attacks are able to query the model and obtain its output, but without the knowledge of internal details [14]. These approaches are in line with the popular view in the literature [6]: that the existence of adversarial examples is a *flaw of the model*, that they exist because the model is overly parametrized, nonlinear, etc. According to this reasoning, each model has its own flaws, i.e., its own critical points. Another view is that adversarial examples are consequences of the data distribution on which the model is trained [26]. This would suggest that different models trained on the same data may share some adversarial examples, but they have to be determined in the context of the data distribution.

In this paper, we present a different point of view. We show that it is possible to determine critical points in point clouds from the features of the point cloud itself, without access to the target DNN model or the data distribution. This is referred to as a “no-box” adversarial attack [27]. To our knowledge, our work is the first on no-box attacks in the point cloud literature. In a broader context, no-box attacks suggest that critical points in point clouds are not only consequences of the flaws of deep models, nor the data distribution, but also inherent characteristics of the point clouds themselves, which give them their crucial properties that are important in their analysis, i.e., what makes an airplane - an airplane, or a chair - a chair. In addition to the novel point of view, our methodology

Hanieh Naderi and Shohreh Kasaei are with the Department of Computer Engineering, Sharif University of Technology Tehran, Iran, e-mail: kasaei@sharif.edu.

Chinthaka Dinesh is with Northeastern University, Vancouver, and the School of Engineering Science, Simon Fraser University, Burnaby, BC, Canada, e-mail: c.herathgedara@northeastern.edu.

Ivan V. Bajić is with the School of Engineering Science, Simon Fraser University, Burnaby, BC, Canada, e-mail: ibajic@ensc.sfu.ca.

This work has been supported in part by the Iran National Science Foundation (INSF) and the Natural Sciences and Engineering Research Council (NSERC) of Canada.

leads to a less computationally expensive way of generating adversarial attacks compared to other methods. Furthermore, the attack has the potential to generalize better and be more transferrable to different models, as it is not dependent on any particular target DNN model.

The rest of the paper is organized as follows. The related work is discussed in Section II, together with a more detailed explanation of our contribution. Our proposed methodology is presented in Sections III and IV. The experimental results are reported in Section V, followed by conclusions in Section VI.

II. RELATED WORK

A. Deep models for point cloud analysis

PointNet [28] was a pioneering approach for DNN-based point cloud analysis. Learnt features are extracted from individual points in the input point cloud and then aggregated to global features via max-pooling. As a result of these global features, a shape can be summarized by a sparse set of key points, also called the *critical point set*. The authors of PointNet showed that any set of points between the critical point set and another set called the *upper bound shape* will give the same set of global features, and thus lead to the same network decision. While this proved a certain level of robustness of PointNet to input perturbations, it also pointed to strong reliance on the critical point set, which was subsequently used to design various adversarial attacks.

PointNet has inspired much subsequent work on DNN-based point cloud analysis, of which we review only three approaches subsequently used in our experiments. One of these is PointNet++ [29], a hierarchical network designed to capture fine geometric structures in a point cloud. Three layers make up PointNet++: the sampling layer, the grouping layer, and the PointNet-based learning layer. These three layers are repeated in PointNet++ to learn local geometric structures. Another representative work is Dynamic Graph Convolutional Neural Network (DGCNN) [30]. It exploits local geometric structures by creating a local neighborhood graph and using convolution-like operations on the edges connecting neighboring pairs of points. PointConv [31] is another architecture that extends PointNet by incorporating convolutional layers that work on 3D point clouds. To better handle local features in point cloud data, a multi-layer perceptron (MLP) is used to approximate weight functions, and inverse density scale is used to re-weight these functions.

B. Adversarial attacks on point clouds

Point clouds are defined by the 3D coordinates of points making up the cloud. Thus, adversarial attacks can be performed by adding, dropping, or shifting points in the input cloud. An adversarial attack can be created by examining all points in the input cloud, or just critical points as potential targets. Liu *et al.* [10] were inspired by the success of gradient-guided attack methods, such as Fast Gradient Sign Method (FGSM) [5] and Projected Gradient Descent (PGD) [32], on 2D images. They applied a similar methodology to develop adversarial attacks on 3D point clouds. Similarly, the Carlini and Wagner (C&W) [8] optimization for finding adversarial

examples has also been transplanted to 3D data. For example, Tsai *et al.* [33] use the C&W optimization formulation with an additional perturbation-bound regularization to construct adversarial attacks. To generate an attack with a minimum number of points, Kim *et al.* [34] extend the C&W formulation by adding a term to constrain the number of perturbed points. The adversarial points found in [34] were almost identical to the PointNet critical points.

Xiang *et al.* [11] demonstrated that PointNet can be fooled by shifting or adding synthetic points or adding clusters and objects to the point cloud. To find such adversarial examples, they applied the C&W strategy to the critical points, rather than all points. Constraining the search space around critical points is sometimes necessary because an exhaustive search through an unconstrained 3D space is infeasible. An attack method that uses the critical-point property for PointNet is proposed by Yang *et al.* [22]. By recalculating the class-dependent importance for each remaining point, they iteratively remove the most crucial point for the true class. The authors noted that the critical points exist in different models and that a universal point-dropping method should be developed for all models. Wicker *et al.* [35] proposed randomly and iteratively determining the critical points and then generating adversarial examples by dropping these points.

Arya *et al.* [36] identify critical points by calculating the largest magnitudes of the loss gradient with respect to the points. After finding those points, the authors propose a minimal set of adversarial points among critical points and perturb them slightly to create adversarial examples. Zheng *et al.* [19] developed a more flexible method that extends finding critical points to other deep models besides PointNet. They introduced a *saliency score* defined as

$$s_i = -r_i^{1+\gamma} \frac{\partial \mathcal{L}}{\partial r_i}, \quad (1)$$

where r_i is the distance of the i -th point to the cloud center, γ is a hyperparameter, and $\frac{\partial \mathcal{L}}{\partial r_i}$ is the gradient of the loss \mathcal{L} with respect to the amount of shifting the point towards the center. Adversarial examples are created by shifting the points with high saliency scores towards the center, so that they will not affect the surfaces much.

In addition to the methods for creating adversarial attacks on point clouds, a number of methods for defending against these attacks have been developed [14]. For 3D point cloud classification, adversarial training and point removal as a pre-processing step in training have been extensively studied [37]. Some of the methods proposed for point removal to improve robustness against adversarial attacks include simple random sampling (SRS) [22], statistical outlier removal (SOR) [25], Denoiser and UPsampler Network (DUP-Net) [25], high-frequency removal [24], and salient point removal [10].

C. Our contribution

All existing adversarial attacks on point clouds require, at the very least, access to the target DNN model, so that the output can be examined for various inputs. This is called a *black-box* type of attack. This may give a false sense of security that an attack cannot be created unless the attacker

gains access to the target model. Our present work shows that this is not the case. Specifically, we show that an attack can be created without access to the target DNN model, which is referred to as a *no-box* attack. To our knowledge, this is the first work on no-box attacks in the point cloud literature.

Our focus in this paper is on adversarial drop attacks, with the specific goal of identifying *adversarial drop points* whose removal is likely to change the target model's decision. We start by defining a set of fourteen point cloud features (Section III) derived using concepts from graph signal processing, which represent various characteristics of a point cloud. Using multiple linear regression analysis, we examine which of those features are indicative of adversarial drop points identified using conventional methods (Section IV). Specifically, we examine three DNN models – PointNet [28], PointNet++ [29], and DGCNN [38] – and identify a set of features that have statistically significant influence in predicting adversarial drop points for these models. Then we show that a no-box attack can be created using a combination of these features derived directly from the point cloud. While a no-box attack cannot be more successful than a black-box or white-box attack tailored to a given model, we show that it is significantly better than a random attack. Additionally, we study the transferability of the developed no-box attack to an unseen model, PointConv [31], and examine its effectiveness against different defenses.

III. POINT CLOUD FEATURES

In this section, leveraging recent advances in *graph signal processing* (GSP) [39], [40], we develop a set of fourteen features that represent various characteristics of a point cloud. These features will later be analyzed (Section IV) in terms of their ability to predict adversarial drop points. First, we review the basic concepts in GSP and the graph construction for a given 3D point cloud, which will lead to computing the graph-based features.

A. Preliminaries

1) *Graph definitions*: A undirected weighted graph $\mathcal{G} = (\mathcal{V}, \mathcal{E}, \mathbf{W})$ is defined by a set of N nodes $\mathcal{V} = \{1, \dots, N\}$, edges $\mathcal{E} = \{(i, j)\}$, and a symmetric *adjacency matrix* \mathbf{W} . $W_{i,j} \in \mathbb{R}^+$ is the edge weight if $(i, j) \in \mathcal{E}$, and $W_{i,j} = 0$ otherwise. Diagonal *degree matrix* \mathbf{D} has diagonal entries $D_{i,i} = \sum_j W_{i,j}, \forall i$. A *combinatorial graph Laplacian matrix* \mathbf{L} is defined as $\mathbf{L} \triangleq \mathbf{D} - \mathbf{W}$ [41]. Further, a *transition matrix* \mathbf{A} is defined as $\mathbf{A} \triangleq \mathbf{D}^{-1}\mathbf{W}$ [42]. By definition $\sum_{j \in \mathcal{N}_i} A_{i,j} = 1$. In general, a vector $\mathbf{x} = [x_1 \dots x_N]^\top \in \mathbb{R}^V$ can be interpreted as a graph signal, where x_i is a scalar value assigned to node $i \in \mathcal{V}$. Further, for a given graph signal \mathbf{x} , a weighted average signal value at node i around its neighbors can be computed as

$$\bar{x}_i = (\mathbf{A}\mathbf{x})_i = \sum_{j \in \mathcal{N}_i} A_{i,j}x_j, \quad (2)$$

where \mathcal{N}_i is the 1-hop neighborhoods of node i . Moreover, the second difference of the graph signal \mathbf{x} at node i is given as

$$\tilde{x}_i = (\mathbf{L}\mathbf{x})_i = L_{i,i}x_i + \sum_{j \in \mathcal{N}_i} L_{i,j}x_j. \quad (3)$$

2) *Graph construction for a 3D point cloud*: To enable graph-based feature-extraction of n 3D points, we first construct a neighborhood graph. In particular, we construct an undirected positive graph $\mathcal{G} = (\mathcal{V}, \mathcal{E}, \mathbf{W})$ composed of a node set \mathcal{V} of size n (each node represents a 3D point) and an edge set \mathcal{E} specified by $(i, j, W_{i,j})$, where $i \neq j, i, j \in \mathcal{V}$ and $W_{i,j} \in \mathbb{R}^+$. We connect each 3D point (graph node) to its k nearest neighbors j in Euclidean distance, so that each point can be filtered with its k neighboring points under a graph-structured data kernel [41], [43].

In the graph-based point cloud processing literature [44]–[47], using pairwise Euclidean distance $\|\mathbf{p}_i - \mathbf{p}_j\|_2^2$ to compute edge weight $W_{i,j}$ between nodes i and j is popular, *i.e.*,

$$W_{i,j} = \exp\left\{-\frac{\|\mathbf{p}_i - \mathbf{p}_j\|_2^2}{\sigma^2}\right\}, \quad (4)$$

where $\mathbf{p}_i \in \mathbb{R}^3$ is the 3D coordinate of point i and σ is a parameter. In numerous graph-based point cloud processing works [44]–[46], [48]–[52], σ was manually chosen so that edge weight $W_{i,j}$ is large (close to 1) if 3D points i, j are physically close, and small (close to 0) otherwise.

B. Graph-based feature extraction

Based on these notions, we compute three sets of features for each 3D point in a given point cloud as follows.

1) *3D point coordinates-based features*: A point cloud $\mathbf{P} \in \mathbb{R}^{n \times 3}$ is a set of n points in a 3D space, $\mathbf{P} = [\mathbf{p}_i], i = 1, 2, \dots, n$, where each point, $\mathbf{p}_i = (p_{x,i}, p_{y,i}, p_{z,i})$, is represented by its x-y-z coordinates. The point cloud can also be represented as $\mathbf{P} = [\mathbf{p}_x; \mathbf{p}_y; \mathbf{p}_z]$, where $\mathbf{p}_x, \mathbf{p}_y$, and \mathbf{p}_z are the n -dimensional column-vectors representing x -, y -, and z -coordinates. Here, we consider $\mathbf{p}_x, \mathbf{p}_y$, and \mathbf{p}_z as three graph signals on graph \mathcal{G} constructed from a given point cloud as in Section III-A2. Therefore, using (2), one can easily compute the weighted average 3D coordinate at node i as follows:

$$\bar{\mathbf{p}}_i = \left((\mathbf{A}\mathbf{P})^\top\right)(:, i) = \sum_{j \in \mathcal{N}_i} A_{i,j}\mathbf{p}_j, \quad (5)$$

where $\left((\mathbf{A}\mathbf{P})^\top\right)(:, i)$ is the i -th column of $(\mathbf{A}\mathbf{P})^\top$. Further, according to (3), we can write the second difference of 3D coordinates \mathbf{P} at node i as follows:

$$\tilde{\mathbf{p}}_i = \left((\mathbf{L}\mathbf{P})^\top\right)(:, i) = L_{i,i}\mathbf{p}_i + \sum_{j \in \mathcal{N}_i} L_{i,j}\mathbf{p}_j. \quad (6)$$

Now, we consider x -, y -, and z -coordinates $\bar{\mathbf{p}}_i$ and $\tilde{\mathbf{p}}_i$ are one set of graph-based features at point i .

2) *Local variation-based features*: Similar to [42], local variation at point i can be quantified as:

$$v_i = \|\mathbf{p}_i - \bar{\mathbf{p}}_i\|_2, \quad (7)$$

where $\bar{\mathbf{p}}_i$ is in (5). Here, one can easily see that v_i is the Euclidean distance between point \mathbf{p}_i and the weighted average of its neighbors. Therefore, when the value of v_i is high, the point p_i cannot be well approximated from those of its neighboring points, and hence the point \mathbf{p}_i is thus likely to be a point of an edge, corner, or valley.

Further, we consider $\mathbf{v} = [v_1 \dots v_n]^\top$ as a graph signal of the graph \mathcal{G} constructed from the given point cloud as discussed in Section III-A2. Then, according to (2), weighted average signal value at node i is given as:

$$\bar{v}_i = \sum_{j \in \mathcal{N}_i} A_{i,j} v_j. \quad (8)$$

Using (3), second difference of signal \mathbf{v} at node i is given as:

$$\tilde{v}_i = L_{i,i} v_i + \sum_{j \in \mathcal{N}_i} L_{i,j} v_j. \quad (9)$$

Now, we consider v_i , \bar{v}_i and \tilde{v}_i are the second set of graph-based features at point i .

3) *Low-pass filter-based features*: For graph signals $\mathbf{p}_x, \mathbf{p}_y, \mathbf{p}_z$ with respect to the graph \mathcal{G} , the corresponding *low-pass filter* (LPF) signals $\mathbf{q}_x^*, \mathbf{q}_y^*, \mathbf{q}_z^*$ can be obtained by minimizing the following optimization problem (See [53] for details):

$$\mathbf{q}^* = \arg \min_{\mathbf{q}} \|\mathbf{p} - \mathbf{q}\|_2^2 + \gamma (\mathbf{q}_x^\top \mathbf{L} \mathbf{q}_x + \mathbf{q}_y^\top \mathbf{L} \mathbf{q}_y + \mathbf{q}_z^\top \mathbf{L} \mathbf{q}_z), \quad (10)$$

where $\mathbf{q}^* = [(\mathbf{q}_x^*)^\top (\mathbf{q}_y^*)^\top (\mathbf{q}_z^*)^\top]^\top$, $\mathbf{q} = [\mathbf{q}_x^\top \mathbf{q}_y^\top \mathbf{q}_z^\top]^\top$, $\mathbf{p} = [\mathbf{p}_x^\top \mathbf{p}_y^\top \mathbf{p}_z^\top]^\top$, and $\gamma > 0$ is a regularization parameter. Since (10) is a *quadratic programming* (QP) problem, its solution can be obtained by solving the following system of linear equations:

$$(\mathbf{I} + \gamma \bar{\mathbf{L}}) \mathbf{q}^* = \mathbf{p}, \quad (11)$$

where $\bar{\mathbf{L}} = \text{diag}\{\mathbf{L}, \mathbf{L}, \mathbf{L}\}$. Since \mathbf{L} is a *positive semi-definite* (PSD) matrix by definition [54], one can easily see that $\bar{\mathbf{L}}$ is also a PSD matrix. Hence $(\mathbf{I} + \gamma \bar{\mathbf{L}})$ is a *positive definite* (PD) matrix for $\gamma > 0$ and thus invertible.

Moreover, we define another graph signal $\mathbf{h} = [h_1 \dots h_n]$, where $h_i = \|\mathbf{p}_i - \mathbf{q}_i^*\|_2$. Here, $\mathbf{q}_i^* \in \mathbb{R}^3$ is x, y, z coordinates of the LPF coordinates at point i obtained from (11). Further, similar to (8) and (9), we can compute the weighted average signal value at node i and the second difference of \mathbf{h} at node i (denoted as \bar{h}_i and \tilde{h}_i , respectively.) Then, we consider h_i, \bar{h}_i and \tilde{h}_i are the third set of graph-based features at point i .

In addition to the aforementioned graph-based features, we compute the following two features for each point i :

- 1) Euclidean distance between point i and the centroid of the corresponding point cloud.
- 2) The number of points inside a ball of radius r and center \mathbf{p}_i . In this paper, we manually choose $r = 0.1$.

Altogether, we have created fourteen features (denoted as $\{f_j^i | j = 1, \dots, 14\}$) for any given point i , as summarized in Table I. These are: the edge intensity value (f_1^i), weighted average of 3D coordinates around neighboring points (f_2^i, f_3^i, f_4^i), second difference of 3D coordinates (f_5^i, f_6^i, f_7^i), the weighted average of edge intensity values around neighboring points (f_8^i), the second difference of edge intensity values (f_9^i), the distance from the centroid (f_{10}^i), the number of points inside a ball of radius $r = 0.1$ (f_{11}^i), the distance between actual 3D points and the low-pass-filtered (LPF) 3D points (f_{12}^i), the weighted average of LPF distance around neighbors (f_{13}^i) and the second difference of LPF distance (f_{14}^i).

IV. FEATURE ANALYSIS AND NO-BOX ATTACK

In this section, we present a methodology that allows us to examine how well the features introduced in Section III are able to predict adversarial drop points. First, each point is assigned an *adversarial score* that reflects how much it contributes to the corresponding model's prediction. Then, multiple linear regression is used to examine how predictive are various features of the adversarial score.

A. Adversarial score

Let $F : \mathbb{R}^{n \times 3} \rightarrow \{1, 2, \dots, C\}$ be a trained C -class classifier, which maps an input point cloud \mathbf{P} to a class $c_t \in \{1, 2, \dots, C\}$, such that $F(\mathbf{P}) = c_t$. An adversarial attack aims to deceive the classifier by changing the point cloud \mathbf{P} to \mathbf{P}^{adv} so that $F(\mathbf{P}^{adv}) \neq c_t$, while usually also requiring $\mathbf{P}^{adv} \approx \mathbf{P}$.

Saliency score (1) is an indicator of the sensitivity of the classifier to a perturbation of an input point. It has been shown [19] to be effective in determining adversarial points, in the sense that perturbing or removing points with high saliency score can create adversarial examples. One issue with the saliency score is that its dynamic range can be variable. Hence, we define our adversarial score by normalizing the saliency score to the range $[0, 1]$. Specifically, for the i -th point \mathbf{p}_i , we define the adversarial score as

$$z(\mathbf{p}_i) = \frac{s_i - \min\{s_1, \dots, s_n\}}{\max\{s_1, \dots, s_n\} - \min\{s_1, \dots, s_n\}}, \quad (12)$$

where s_i is given in (1). In the next section, we examine how well our fourteen features are able to predict $z(\mathbf{p}_i)$.

B. Multiple linear regression

We employ multiple linear regression analysis [55], [56] to examine how predictive are the features defined in Section III of the adversarial score $z(\mathbf{p}_i)$ in (12). Note that this idea may seem strange to start with: $z(\mathbf{p}_i)$ depends on the classifier model, via the loss \mathcal{L} in the saliency score s_i in (1), while the features in Section III do not! Yet, as the results will show, some of our features are fairly predictive of $z(\mathbf{p}_i)$.

For a given point \mathbf{p}_i , its adversarial score $z(\mathbf{p}_i)$ and its features $\{f_j^i | j = 1, \dots, 14\}$, we set up the following multiple linear regression model:

$$z(\mathbf{p}_i) \approx \sum_{j=1}^{14} c_j \cdot f_j^i, \quad (13)$$

where c_j are the regression coefficients. An illustration is shown in Fig. 1. The coefficients will be fitted on a set of points from a dataset of point clouds. Naturally, there is a variation in the coefficient values across different point clouds. To determine whether a particular feature is predictive of $z(\mathbf{p}_i)$, we run the following hypothesis test for each coefficient c_j as a t-test [55]:

$$\begin{aligned} H_0 : c_j &= 0, \\ H_1 : c_j &\neq 0. \end{aligned} \quad (14)$$

Here, the null hypothesis H_0 is $c_j = 0$. If the null hypothesis cannot be rejected for a particular coefficient c_j , it means that,

Table I: Fourteen features created for the i -th point in a given point cloud.

Feature symbol	Explanation
f_1^i	v_i . See (7) and Section III-B2.
f_2^i	x coordinate of $\bar{\mathbf{p}}_i$. See (5) and Section III-B1.
f_3^i	y coordinate of $\bar{\mathbf{p}}_i$. See (5) and Section III-B1.
f_4^i	z coordinate of $\bar{\mathbf{p}}_i$. See (5) and Section III-B1.
f_5^i	x coordinate of $\tilde{\mathbf{p}}_i$. See (6) and Section III-B1.
f_6^i	y coordinate of $\tilde{\mathbf{p}}_i$. See (6) and Section III-B1.
f_7^i	z coordinate of $\tilde{\mathbf{p}}_i$. See (6) and Section III-B1.
f_8^i	\bar{v}_i . See (8) and Section III-B2.
f_9^i	\tilde{v}_i . See (9) and Section III-B2.
f_{10}^i	Euclidean distance between point i and the centroid of the point cloud.
f_{11}^i	The number of points inside a ball of radius r and center \mathbf{p}_i .
f_{12}^i	h_i . See Section III-B3.
f_{13}^i	\bar{h}_i . See Section III-B3.
f_{14}^i	\tilde{h}_i . See Section III-B3.

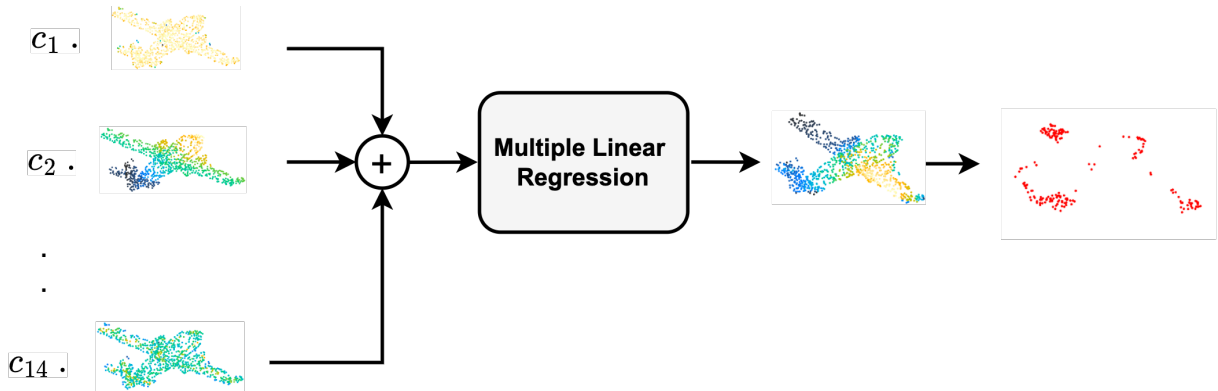


Figure 1: An overview of multiple linear regression analysis. Fourteen features are computed for each point in the point cloud. In the figure, feature values are represented with different colors, with black corresponding to high values and light yellow corresponding to low values. At each point, features are linearly combined using the coefficients estimated on the training data, whose significance is determined using statistical testing. In the final experiment, the N points with the highest predicted score are compared against the N points with the highest true adversarial score.

given the variation, the coefficient is not significantly different from zero. The interpretation would be that the corresponding feature f_j^i does not contribute significantly to the prediction of the adversarial score $z(\mathbf{p}_i)$. On the other hand, for coefficients c_j where the null hypothesis can be rejected, we can conclude that the corresponding feature f_j^i is statistically significantly predictive of $z(\mathbf{p}_i)$. As will be seen in Section V, some features are predictive of $z(\mathbf{p}_i)$, others are not.

C. No-box drop attack

Let $\mathcal{F} \subseteq \{1, 2, \dots, 14\}$ be the set of indices of features that have been determined to have a statistically significant effect on the adversarial score, as described in Section IV-B. For each point \mathbf{p}_i in a given point cloud \mathbf{P} , we compute the predicted adversarial score using the statistically significant features as

$$\hat{z}(\mathbf{p}_i) = \sum_{j \in \mathcal{F}} c_j \cdot f_j^i, \quad (15)$$

where c_j is the coefficient of the j -th feature estimated through multiple linear regression analysis. Note that $z(\mathbf{p}_i)$ is the true

adversarial score obtained from (1) and (12), which requires access to the target DNN model, while $\hat{z}(\mathbf{p}_i)$ is the predicted adversarial score computed from the point cloud itself, and does not require access to the target DNN model. Once the predicted adversarial scores $\hat{z}(\mathbf{p}_i)$ are computed for all points in the point cloud, the points are sorted in decreasing order of $\hat{z}(\mathbf{p}_i)$. To create a drop- N attack, the top N points on the sorted list are removed from the point cloud.

V. EXPERIMENTS

A. Experimental setting

We used the aligned benchmark ModelNet40¹ dataset, which contains 40 object classes. The dataset that was used in our study consists of 9,843 training and 2,468 test point clouds. Each point cloud contains 1,024 points. For start, three models – PointNet, PointNet++, and DGCNN, with implementation from [23] – were used as deep classifiers

¹<https://github.com/kimianoorbakhsh/LPF-Defense/tree/main/model/Data>

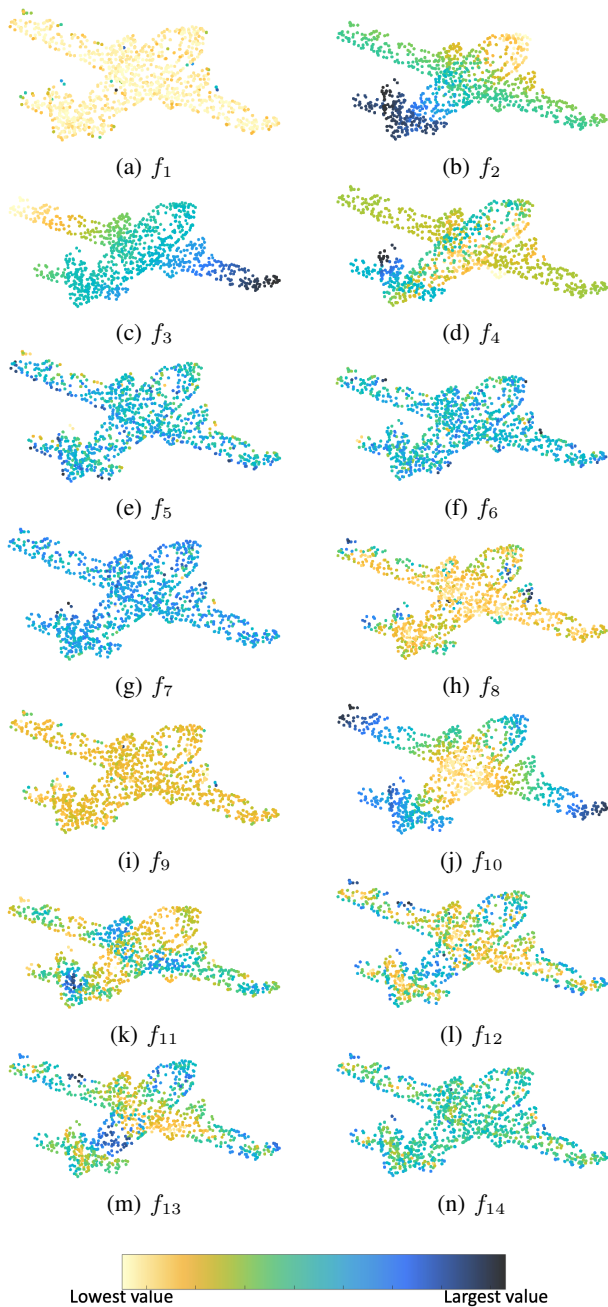


Figure 2: Visualization of 14 features. Points are colored by the feature value at each point, according to the shown color map.

on the ModelNet40 dataset. Subsequently, another model, PointConv [31], was used to test attack transferability. The approach from [19] was used to compute saliency scores (1) iteratively. Specifically, [19] was used to compute the saliency scores for the initial point cloud, then 10 points with the highest score were removed, then this was repeated for the remaining points until a total of N points were identified. Once the N points with the highest saliency score were identified, their adversarial score $z(\mathbf{p}_i)$ was computed as in (12). All experiments were conducted using PyTorch on a machine with a NVIDIA Tesla P100-PCIe card with 16 GB of memory.

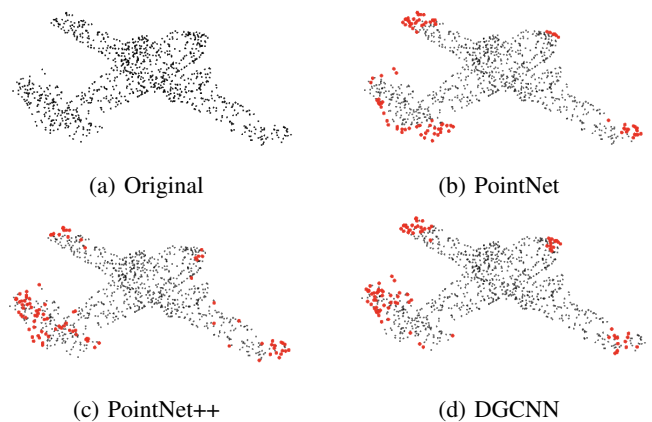


Figure 3: Illustration of adversarial points on the airplane object (a); sub-figures (b), (c), and (d) show the 100 points with the highest adversarial score obtained using the corresponding network.

B. Multiple linear regression analysis

Fig. 2 shows a visualization of the fourteen features defined in Section III on the airplane object. Each point’s color reflects the value of the corresponding feature at that point, with dark blue indicating high values and light yellow indicating low values.

Saliency scores s_i in (1), and therefore also the adversarial scores $z(\mathbf{p}_i)$ in (12), tend to be most reliable when s_i is high. Therefore, we applied multiple linear regression analysis only to the N points with the highest scores, where $N \in \{50, 100, 150, 200\}$. Fig. 3 shows a visualization of the 100 points with the highest adversarial score, computed from saliency scores of three models: PointNet, PointNet++, and DGCNN. An interesting observation is that, while each network is different, adversarial points tend to cluster in specific regions like the tail, wings, and tips. Comparing Figs. 2 and 3, we can also see that some features might be indicative of the adversarial points.

To formally test this idea, we use multiple linear regression analysis, specifically the `scikit-learn`² implementation. For each object in the training set, we select N points with the highest adversarial score $z(\mathbf{p}_i)$, then fit the regression model (13). Hypothesis test (14) is run for each coefficient c_j to see whether the null hypothesis can be rejected at the significance level of $\alpha = 0.05$ [55]. Those coefficients for which the null hypothesis can be rejected are deemed significantly different from zero, and the corresponding feature is regarded as sufficiently explanatory for $z(\mathbf{p}_i)$. Other coefficients, for which the null hypothesis cannot be rejected at the significance level of $\alpha = 0.05$, are deemed insignificant, and the corresponding features regarded as not sufficiently explanatory for $z(\mathbf{p}_i)$. This procedure is repeated for $N \in \{50, 100, 150, 200\}$. The results are shown in Tables II, III, and IV for PointNet, PointNet++, and DGCNN, respectively, where insignificant coefficients are shown as 0.

²<https://scikit-learn.org/stable/>

Table II: Multiple linear regression analyses for $N \in \{50, 100, 150, 200\}$ points with the highest adversarial score derived from PointNet. Significant coefficients (at $\alpha = 0.05$) are shown with 3 decimal points precision, while insignificant coefficients are shown as 0.

N	c_1	c_2	c_3	c_4	c_5	c_6	c_7	c_8	c_9	c_{10}	c_{11}	c_{12}	c_{13}	c_{14}	R^2 (%)
50	-38.043	0.007	0.005	-0.009	0	0	0	0	4.659	0.648	0.011	-3.554	12.309	0.196	94.3%
100	-44.032	0.007	0.006	-0.008	0	0	0	0	5.113	0.636	0.011	-3.139	11.733	0.164	94.2%
150	-42.295	0.007	0.006	-0.007	0	0	0	0	4.904	0.623	0.010	-3.055	11.470	0.160	94.1%
200	-41.451	0.007	0.005	-0.007	0	0	0	0	4.819	0.611	0.010	-2.969	11.207	0.153	93.9%

Table III: Multiple linear regression analyses for $N \in \{50, 100, 150, 200\}$ points with the highest adversarial score derived from PointNet++. Significant coefficients (at $\alpha = 0.05$) are shown with 3 decimal points precision, while insignificant coefficients are shown as 0.

N	c_1	c_2	c_3	c_4	c_5	c_6	c_7	c_8	c_9	c_{10}	c_{11}	c_{12}	c_{13}	c_{14}	R^2 (%)
50	-54.854	0.009	0.006	-0.007	0	0	0	8.859	6.112	0.649	0.011	-2.665	11.375	0.122	94.3%
100	-49.452	0.008	0.005	-0.007	0	0	0	6.851	5.544	0.636	0.010	-2.908	11.370	0.148	94.2%
150	-44.927	0.008	-0.006	-0.008	0	0	0	3.120	5.125	0.624	0.010	-3.067	11.320	0.161	94.1%
200	-43.109	0.007	0.005	-0.007	0	0	0	2.489	4.938	0.612	0.010	-3.057	11.091	0.163	93.9%

Table IV: Multiple linear regression analyses for $N \in \{50, 100, 150, 200\}$ points with the highest adversarial score derived from DGCNN. Significant coefficients (at $\alpha = 0.05$) are shown with a precision of 3 decimal points, while insignificant coefficients are shown as 0.

N	c_1	c_2	c_3	c_4	c_5	c_6	c_7	c_8	c_9	c_{10}	c_{11}	c_{12}	c_{13}	c_{14}	R^2 (%)
50	-52.555	0.006	0.006	-0.008	0	0	0	10.169	5.870	0.648	0.011	-3.058	11.745	0.157	94.4%
100	-46.105	0.006	0.005	-0.007	0	0	0	4.473	5.241	0.636	0.011	-3.257	11.818	0.177	94.3%
150	-43.374	0.007	0.005	-0.007	0	0	0	3.352	4.960	0.623	0.011	-3.179	11.540	0.173	94.2%
200	-41.795	0.006	0.004	-0.007	0	0	0	3.585	4.806	0.610	0.011	-3.153	11.330	0.174	94.0%

Consider Table II first. Four coefficients are insignificant: c_5 , c_6 , c_7 , and c_8 , and these are shown as 0, while the others are significant at $\alpha = 0.05$. The last column contains the R^2 coefficient of determination [55], shown as a percentage. We can see that R^2 is around 94%, which is fairly high and indicates good agreement between the data and the model. As the number of points N increases, it becomes harder for the model to fit the data, hence the drop in R^2 . Similar behavior can be seen in Tables III and IV as well, although in these cases, c_8 is significant.

Another observation is that there is a large overlap between the set of significant coefficients for PointNet, PointNet++, and DGCNN, even though these DNN models are quite different. This suggests that certain features of the point cloud itself may be able to predict adversarial points for different DNN models, and this is what makes “no-box” attacks possible. Specifically, we see that edge intensity (f_1), weighted coordinate-based features (f_2 , f_3 , f_4), local variation-based feature (f_9), distance from the centroid (f_{10}), and LPF-based features (f_{11} , f_{12} , f_{13} , f_{14}) are all indicative of the adversarial score for all three DNN models.

Tables II, III, and IV also give the coefficients of the linear combination of features that best predicts the adversarial score for each case. For example, if we were to predict the adversarial score derived from PointNet for the top $N = 150$ points, then based on the corresponding row in Table II, we could use the following linear model:

$$\begin{aligned}
\mathfrak{z}(\mathbf{p}_i) = & -42.295 \cdot f_1^i + 0.007 \cdot f_2^i + 0.006 \cdot f_3^i \\
& - 0.007 \cdot f_4^i + 4.904 \cdot f_9^i + 0.623 \cdot f_{10}^i \\
& + 0.010 \cdot f_{11}^i - 3.055 \cdot f_{12}^i + 11.470 \cdot f_{13}^i \\
& + 0.160 \cdot f_{14}^i.
\end{aligned} \tag{16}$$

Although the best coefficients are different for different cases (i.e., different N 's and tables), it is noticeable that the coefficient values do not change too much - they are the same order of magnitude across all cases. It can also be observed from Tables II, III, and IV that the regression coefficients do not vary greatly across the different cases, regardless of whether the linear model was fit to the adversarial scores from PointNet, PointNet++, or DGCNN. This consistency in the coefficient values suggests that the features identified as significant by the regression analysis are robust predictors of adversarial points, regardless of the DNN model. We test this observation in subsequent experiments in Sections V-C and V-D.

To examine how accurately the regression model predicts the true adversarial scores, we show four graphs in Fig. 4. These graphs correspond to four point clouds whose adversarial scores were computed based on PointNet. The blue scatter plots show $N = 100$ points as pairs of values (Predicted, True), where Predicted is the adversarial score $\mathfrak{z}(\mathbf{p}_i)$ predicted by the linear model (13), while True is the true adversarial score $z(\mathbf{p}_i)$ from (12). Ideally, if the predictions were perfect, all the blue points would fall on the straight red line. Although this is not the case in practice, we see that they are close and, more importantly, that the rank order is mostly preserved. This means that if we were looking for the N points with the highest true adversarial score, we could find many of them by computing the predicted score from the features and taking N points with the highest predicted score.

To test this idea further, we compute the overlap between the set of top- N points according to the true adversarial score $z(\mathbf{p}_i)$ from (12) and the set of top- N points according to the predicted adversarial score $\mathfrak{z}(\mathbf{p}_i)$ from (13). The results

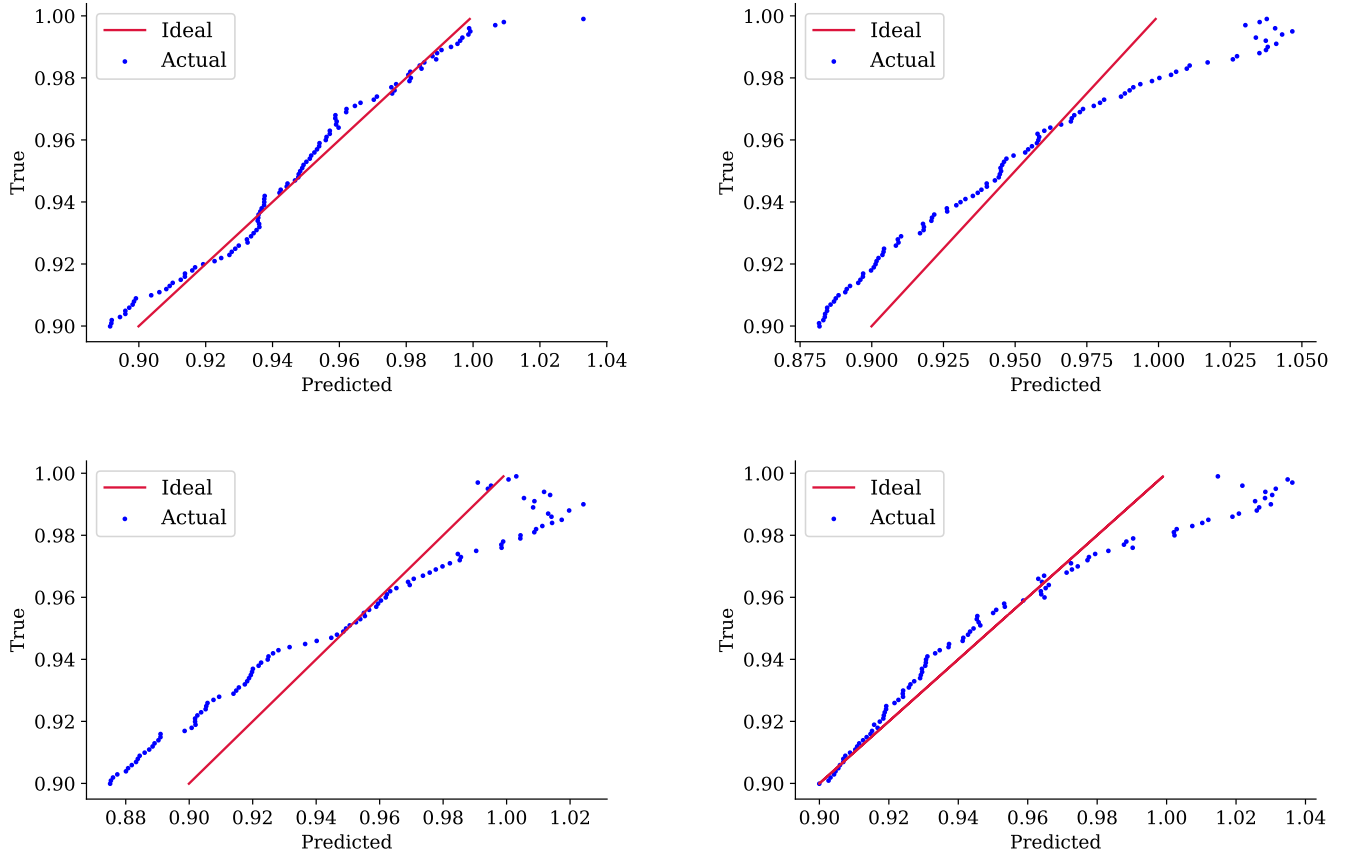


Figure 4: Predicted vs. true adversarial scores for four point clouds. A perfect prediction would correspond to the straight red line, actual predictions give blue scatter plots.

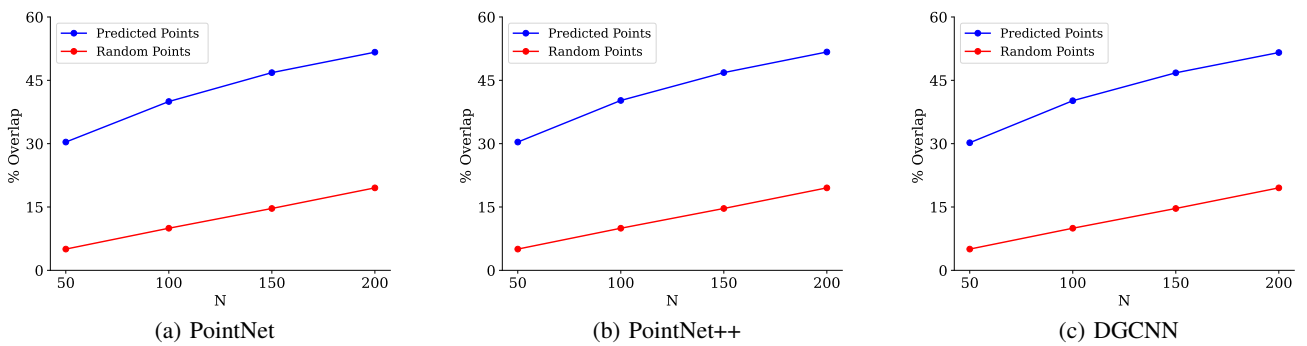


Figure 5: Percentage overlap between top- N points with predicted and true adversarial scores generated by (a) PointNet, (b) PointNet++, and (c) DGCNN. Overlap with randomly chosen points is also shown.

are shown in Fig. 5. The three graphs correspond to the three networks (PointNet, PointNet++, and DGCNN) based on which the true adversarial scores are computed. Each graph shows the percentage overlap for $N \in \{50, 100, 150, 200\}$, for the prediction based on proposed features, as well as a random selection of points. The gap between the two lines indicates how much better is the prediction based on the proposed features compared to a random guess. As seen in the graphs, the prediction based on the proposed features is about 25-30% better than a random guess and achieves over 50% overlap with the true adversarial drop points for $N = 200$.

C. Attack success rate

The attack success rate measures how effective a particular adversarial attack is at fooling the target deep model. The attack success rate is typically reported as a percentage of cases in which the target model was fooled on a given dataset, with a higher number indicating a more successful attack. In the next experiment, we examine the attack success rates on the ModelNet40 test set.

Since there are no existing no-box attacks on 3D point cloud classification, we pick as our “Baseline” method a white-box attack based on saliency score (1), which is the un-normalized version of the true adversarial score (12). The “Baseline” attack involves dropping 100 or 200 points with the highest true saliency scores. This is a white-box attack and requires access to the target DNN model so that gradients relative to the loss function can be computed in (1). Although the white-box attack clearly has an advantage over the proposed no-box attack, the comparison still helps us gain insight into how much the attack success rate can be improved by having access to the target DNN model. The second method (“Proposed”) is the proposed no-box attack, which drops 100 or 200 points with the highest predicted adversarial score $\mathfrak{z}(\mathbf{p}_i)$ from (15), using the *averaged* significant coefficients from Tables II, III, and IV. The purpose of using the average coefficients from the three tables is to avoid having the prediction model (15) be fitted to any particular target DNN. The third method (“Random”) drops 100 or 200 randomly selected points.

Table V shows the attack success rate results. Note that the table also includes results for PointConv [31], a model that was not included in the computation of coefficients in Tables II, III, and IV. As expected, the Baseline method achieves the highest success rate, since it is a white-box attack that uses a particular target DNN model to figure out which points are the most important for that model. However, the Proposed method, although it is a no-box attack, comes fairly close on PointNet++, DGCNN, and PointConv, with differences in the range of 2–4% on the Drop100 attack; it is also much better than the Random drop attack. The Proposed approach does not need access to the target DNN model and does not make any assumptions about the internal structure of the model. Moreover, its performance across different DNN models is fairly consistent; its attack success rates vary by up to 5% for Drop100 and 13% for Drop200 across different DNN models. Meanwhile, the Baseline’s success rate varies by 20% for Drop100 across different DNNs, and over 30% for

Drop200. This indicates better generalization of the Proposed method compared to the Baseline approach, even if its success rate is not as high.

D. Transferability

When adversarial points are determined for a particular DNN model, it is natural to ask whether the same adversarial points could create a successful attack on another DNN model. The ability to transfer an attack from one DNN model to another is an important aspect to consider when evaluating the robustness of an attack strategy. In the next experiment, we examine how well the adversarial points for the Drop100 attack identified on one DNN model (“source”) work on another DNN model (“target”). What this means for the Proposed attack is that the coefficients of the linear model (13) are fitted on the source model and then used to predict adversarial drop points on the target model.

Table VI shows the transferability results in terms of the success rate of the Drop100 attack on the ModelNet40 test set. When the source and target models match, the Baseline approach has a higher success rate than the Proposed method, as expected. However, the success rate of the Baseline approach drops significantly when the target is different from the source. For example, there is more than a 20% drop in the success rate of the Baseline attack when the source model is PointNet and the target is changed to any of the other three models. Meanwhile, the success rate of the Proposed approach also degrades when the source and target models are not the same, but this degradation is much smaller than with the Baseline approach. In fact, the success rate of the Proposed method is higher than the Baseline when the source and target models differ. Overall, the Proposed approach exhibits higher transferability and a more predictable performance against an unknown target model.

E. Performance of various defenses

Next, we test the performance of several defenses – SRS [22], SOR [25], DUP-Net [25], and If-Defense [23] – against the Baseline and Proposed Drop100 attacks. Here, the Proposed attack is based on the averaged significant coefficients from Tables II, III, and IV. The target model is PointConv, which was not used in the computation of coefficients in Tables II, III, and IV. Table VII shows the classification accuracy of PointConv under different attacks and defenses. For reference, the “No-attack” column shows the accuracy when there is no attack. The lower classification accuracy indicates that the attack is more successful. We see from the table that defenses are successful to varying degrees, with If-Defense being the most successful in keeping the classification accuracy high. The classification accuracies under the two attacks are fairly similar, deviating by only 1-4%. While the Baseline attack performs better under weaker defenses, the Proposed attack proves slightly better under the strongest defenses, specifically DUP-Net and If-Defense. Overall, we could say that against four popular defenses, the Proposed no-box attack achieves a comparable performance to the Baseline white-box attack, despite not having access

Table V: Comparison of the Baseline, Proposed, and Random attacks in terms of attack success rate.

Model	Attacks					
	Baseline		Proposed (averaged coefficients)		Random	
	Drop100 [19]	Drop200 [19]	Drop100	Drop200	Random Drop100	Random Drop200
PointNet [28]	39.98	66.97	21.80	38.13	13.82	14.10
PointNet++ [29]	19.72	38.17	17.49	25.66	11.67	11.39
DGCNN [38]	25.46	43.47	22.07	35.11	10.23	11.33
PointConv [31]	22.01	35.86	18.09	30.09	11.01	11.89

Table VI: Transferability of Drop100 attacks in terms of attack success rate.

Source DNN Model	Drop100 Attack	Target DNN model			
		PointNet [28]	PointNet++ [29]	DGCNN [38]	PointConv [31]
PointNet [28]	Baseline [19]	39.98	17.91	17.00	15.61
	Proposed (coefficients)	25.40	20.12	21.07	20.31
PointNet++ [29]	Baseline [19]	14.21	19.72	12.27	10.36
	Proposed (coefficients)	17.00	17.80	16.96	15.45
DGCNN [38]	Baseline [19]	18.47	18.97	25.46	17.52
	Proposed (coefficients)	20.77	20.85	22.07	19.55
PointConv [31]	Baseline [19]	11.93	12.88	15.25	22.01
	Proposed (coefficients)	16.33	16.73	17.66	21.61

to the target DNN model. This makes it a fairly robust and universal approach for generating adversarial attacks on point cloud analysis models.

F. Computational cost

Next, we compare the computational cost of generating the Baseline and Proposed Drop100 attack. Again, the Proposed attack is based on the averaged significant coefficients from Tables II, III, and IV. The experiment was carried out in a Google Colab environment using a NVIDIA Tesla T4 GPU. Table VIII shows the average run time in seconds per point cloud needed to generate an attack, averaged over the ModelNet40 test set. As seen in the table, the Proposed attack is approximately **23 times** faster than the Baseline. This is due to its no-box nature, which allows it to generate the attack directly from the point cloud, without having to pass gradients through the target DNN model.

G. Visualizations

Finally, we show several visualizations of true and predicted adversarial drop points in Fig. 6. The 100 points with the highest adversarial score $z(\mathbf{p}_i)$ from (12), computed based on PointNet, are shown in red on the three point clouds on the left, while other points are shown in gray. The middle column shows the 100 points with the highest predicted adversarial score $\hat{z}(\mathbf{p}_i)$ computed from (15), with the coefficients from Table II for $N = 100$. Compared with the red points in the three clouds on the left, we see a very good agreement. For example, true and predicted adversarial points tend to concentrate near the chair legs and edges of the seat (top cloud), tip and sides of the cone (middle cloud), legs and corners (bottom cloud). The last column highlights 100 randomly selected points, which are spread all over the corresponding clouds. Clearly, the predicted adversarial points are much closer to the true adversarial points than a random guess.

VI. CONCLUSION

Black-box and white-box adversarial attacks on 3D point clouds require access to the target DNN model in order to

create an adversarial example that would fool that model. In this paper, we presented a strategy that does not require the target DNN model in order to create an adversarial example. This is termed a *no-box* attack, and is the first such attack in the point cloud literature. Although no-box attacks cannot be more successful than white- or black-box attacks, since they cannot fine-tune an adversarial example to a particular target model, this work demonstrates that the attacker does not need access to the target model in order to craft an adversarial attack on it. The proposed no-box attack was shown to generalize better, be more transferable, and much faster than a baseline white-box attack. Furthermore, when faced with typical defenses, its success was comparable to that of the baseline white-box attack. One implication of this work is that the geometry of data instances, and not just the architecture of the target model or the data distribution, is important for adversarial attacks, and this insight could help to design better defenses in the future.

REFERENCES

- [1] K. Zhang, W. Zuo, Y. Chen, D. Meng, and L. Zhang, "Beyond a gaussian denoiser: Residual learning of deep CNN for image denoising," *IEEE Trans. Image Processing*, vol. 26, no. 7, pp. 3142–3155, 2017.
- [2] Y. Song, Z. He, H. Qian, and X. Du, "Vision transformers for single image dehazing," *IEEE Trans. Image Processing*, vol. 32, pp. 1927–1941, 2023.
- [3] K. H. Jin, M. T. McCann, E. Froustey, and M. Unser, "Deep convolutional neural network for inverse problems in imaging," *IEEE Trans. Image Processing*, vol. 26, no. 9, pp. 4509–4522, 2017.
- [4] Y. Dong, Q. Liu, B. Du, and L. Zhang, "Weighted feature fusion of convolutional neural network and graph attention network for hyperspectral image classification," *IEEE Trans. Image Processing*, vol. 31, pp. 1559–1572, 2022.
- [5] I. J. Goodfellow, J. Shlens, and C. Szegedy, "Explaining and harnessing adversarial examples," in *Proc. ICLR*, 2015.
- [6] C. Szegedy, W. Zaremba, I. Sutskever, J. Bruna, D. Erhan, I. J. Goodfellow, and R. Fergus, "Intriguing properties of neural networks," in *Proc. ICLR*, 2014.
- [7] S.-M. Moosavi-Dezfooli, A. Fawzi, O. Fawzi, and P. Frossard, "Universal adversarial perturbations," in *Proc. IEEE/CVF CVPR*, 2017, pp. 1765–1773.
- [8] N. Carlini and D. Wagner, "Towards evaluating the robustness of neural networks," in *Proc. IEEE Symp. Security and Privacy*, 2017, pp. 39–57.
- [9] H. Naderi, L. Goli, and Sh. Kasaei, "Generating unrestricted adversarial examples via three parameters," *Multimedia Tools and Applications*, vol. 81, no. 15, pp. 21919–21938, 2022.

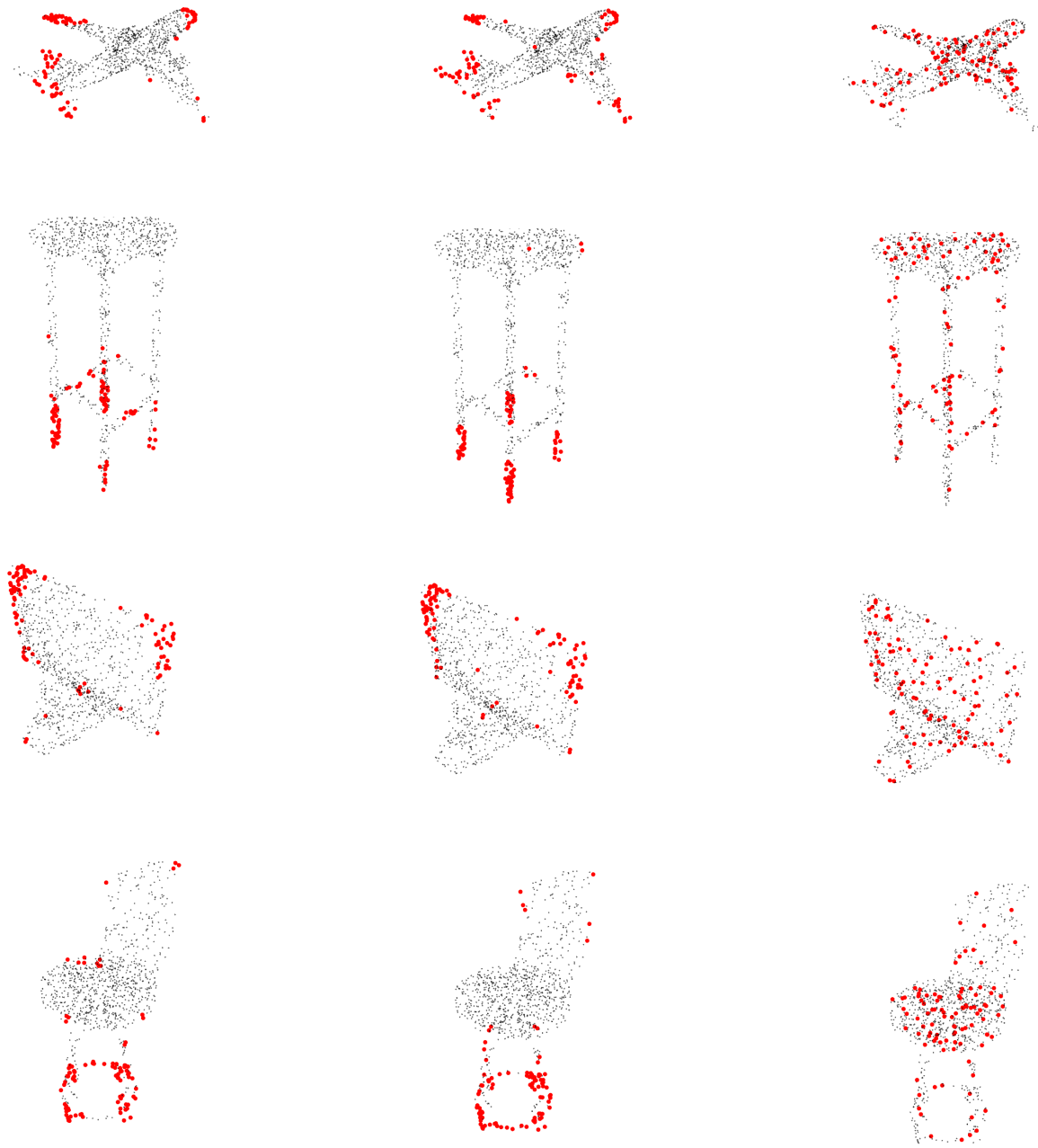


Figure 6: Visualisation of adversarial point prediction, where (predicted) adversarial points are shown in red, and the other points in the cloud as gray. (Left) 100 points with the highest true adversarial score computed based on PointNet. (Middle) 100 points with the highest predicted adversarial score computed using the proposed features. (Right) 100 randomly selected points.

Table VII: Performance of various defenses against Drop100 attacks in terms of PointConv classification accuracy; lower classification accuracy indicates a more successful attack.

Defense	No-attack	Drop100 Attack	
		Baseline	Proposed
No-defense	88.47%	77.99%	81.91%
SRS [22]	84.98%	65.10%	66.00%
SOR [25]	87.26%	69.34%	71.50%
DUP-Net [25]	78.69%	63.75%	63.53%
If-Defense [23]	87.66%	84.42%	84.03%

Table VIII: Average run-time for generating an adversarial point cloud in a Drop100 attack.

Drop100 Attack	Time (s)
Baseline	1.41
Proposed	0.06

- [10] D. Liu, R. Yu, and H. Su, "Extending adversarial attacks and defenses to deep 3D point cloud classifiers," in *Proc. IEEE ICIP*, 2019, pp. 2279–2283.
- [11] C. Xiang, C. R. Qi, and B. Li, "Generating 3D adversarial point clouds," in *Proc. IEEE/CVF CVPR*, 2019, pp. 9136–9144.
- [12] Q. Huang, X. Dong, D. Chen, H. Zhou, W. Zhang, and N. Yu, "Shape-invariant 3D adversarial point clouds," in *Proc. IEEE/CVF CVPR*, 2022, pp. 15335–15344.
- [13] C. Wen, X. Li, H. Huang, Y.-S. Liu, and Y. Fang, "3D shape contrastive representation learning with adversarial examples," *IEEE Trans. Multimedia*, 2023, Early Access.
- [14] H. Naderi and I. V. Bajić, "Adversarial attacks and defenses on 3D point cloud classification: A survey," *IEEE Access*, 2023, Early Access.
- [15] S. Cheng, X. Chen, X. He, Z. Liu, and X. Bai, "PRA-Net: Point relation-aware network for 3D point cloud analysis," *IEEE Trans. Image Processing*, vol. 30, pp. 4436–4448, 2021.
- [16] T. Lu, C. Liu, Y. Chen, G. Wu, and L. Wang, "APP-Net: Auxiliary-point-based push and pull operations for efficient point cloud recognition," *IEEE Trans. Image Processing*, vol. 32, pp. 6500–6513, 2023.
- [17] R. L. de Queiroz and P. A. Chou, "Compression of 3D point clouds using a region-adaptive hierarchical transform," *IEEE Trans. Image Processing*, vol. 25, no. 8, pp. 3947–3956, 2016.
- [18] C. Dinesh, G. Cheung, and I. V. Bajić, "Point cloud denoising via feature graph laplacian regularization," *IEEE Trans. Image Processing*, vol. 29, pp. 4143–4158, 2020.
- [19] T. Zheng, C. Chen, J. Yuan, B. Li, and K. Ren, "Pointcloud saliency maps," in *Proc. IEEE/CVF ICCV*, 2019, pp. 1598–1606.
- [20] B. Zhang, S. Huang, W. Shen, and Z. Wei, "Explaining the PointNet: what has been learned inside the PointNet?," in *Proc. IEEE/CVF CVPR Workshops*, 2019, pp. 71–74.
- [21] S. Fan, W. Gao, and G. Li, "Salient object detection for point clouds," *arXiv preprint arXiv:2207.11889*, 2022.
- [22] J. Yang, Q. Zhang, R. Fang, B. Ni, J. Liu, and Q. Tian, "Adversarial attack and defense on point sets," *arXiv preprint arXiv:1902.10899*, 2021.
- [23] Z. Wu, Y. Duan, H. Wang, Q. Fan, and L. J. Guibas, "If-defense: 3D adversarial point cloud defense via implicit function based restoration," *arXiv preprint arXiv:2010.05272*, 2020.
- [24] H. Naderi, K. Noorbakhsh, A. Etemadi, and Sh. Kasaei, "Lpf-defense: 3d adversarial defense based on frequency analysis," *Plos one*, vol. 18, no. 2, pp. e0271388, 2023.
- [25] H. Zhou, K. Chen, W. Zhang, H. Fang, W. Zhou, and N. Yu, "DUP-Net: denoiser and upsampler network for 3D adversarial point clouds defense," in *Proc. IEEE/CVF ICCV*, 2019, pp. 1961–1970.
- [26] A. Ilyas, S. Santurkar, D. Tsipras, L. Engstrom, B. Tran, and A. Madry, "Adversarial examples are not bugs, they are features," in *Advances in Neural Information Processing Systems*, 2019, pp. 125–136.
- [27] Q. Li, Y. Guo, and H. Chen, "Practical no-box adversarial attacks against DNNs," in *Proc. NeurIPS*, 2020, pp. 12849–12860.
- [28] C. R. Qi, H. Su, K. Mo, and L. J. Guibas, "PointNet: Deep learning on point sets for 3D classification and segmentation," in *Proc. IEEE/CVF CVPR*, 2017, pp. 652–660.
- [29] C. R. Qi, L. Yi, H. Su, and L. J. Guibas, "PointNet++: Deep hierarchical feature learning on point sets in a metric space," *arXiv preprint arXiv:1706.02413*, 2017.
- [30] Y. Wang, Y. Sun, Z. Liu, S. E. Sarma, M. M. Bronstein, and J. M. Solomon, "Dynamic graph CNN for learning on point clouds," *ACM Trans. Graphics*, vol. 38, no. 5, pp. 1–12, 2019.
- [31] W. Wu, Z. Qi, and L. Fuxin, "Pointconv: Deep convolutional networks on 3D point clouds," in *Proc. IEEE/CVF CVPR*, 2019, pp. 9621–9630.
- [32] A. Madry, A. Makelov, L. Schmidt, D. Tsipras, and A. Vladu, "Towards deep learning models resistant to adversarial attacks," *arXiv preprint arXiv:1706.06083*, 2017.
- [33] T. Tsai, K. Yang, T.-Yi Ho, and Y. Jin, "Robust adversarial objects against deep learning models," in *Proceedings of the AAAI Conference on Artificial Intelligence*, 2020, vol. 34, pp. 954–962.
- [34] J. Kim, B.-S. Hua, T. Nguyen, and S.-K. Yeung, "Minimal adversarial examples for deep learning on 3D point clouds," in *Proc. IEEE/CVF ICCV*, 2021, pp. 7797–7806.
- [35] M. Wicker and M. Kwiatkowska, "Robustness of 3D deep learning in an adversarial setting," in *Proc. IEEE/CVF CVPR*, 2019, pp. 11767–11775.
- [36] A. Arya, H. Naderi, and S. Kasaei, "Adversarial attack by limited point cloud surface modifications," *arXiv preprint arXiv:2110.03745*, 2021.
- [37] D. Liu, R. Yu, and H. Su, "Adversarial shape perturbations on 3d point clouds," in *European Conference on Computer Vision Workshops*. Springer, 2020, pp. 88–104.
- [38] A. V. Phan, M. Le Nguyen, Y. L. H. Nguyen, and L. T. Bui, "DGCNN: A convolutional neural network over large-scale labeled graphs," *Neural Networks*, vol. 108, pp. 533–543, 2018.
- [39] D. I. Shuman, S. K. Narang, P. Frossard, Antonio A. Ortega, and P. Vandergheynst, "The emerging field of signal processing on graphs: Extending high-dimensional data analysis to networks and other irregular domains," *IEEE Signal Process. Mag.*, vol. 30, no. 3, pp. 83–98, 2013.
- [40] X. Liu, G. Cheung, X. Wu, and D. Zhao, "Random walk graph laplacian-based smoothness prior for soft decoding of jpeg images," *IEEE Trans. Image Process.*, vol. 26, no. 2, pp. 509–524, Feb 2017.
- [41] A. Ortega, P. Frossard, J. Kovacevic, J. M. F. Moura, and P. Vandergheynst, "Graph signal processing: Overview, challenges, and applications," *Proc. IEEE*, vol. 106, no. 5, pp. 808–828, May 2018.
- [42] S. Chen, D. Tian, C. Feng, A. Vetro, and J. Kovacevic, "Fast resampling of three-dimensional point clouds via graphs," *IEEE Trans. Signal Process.*, vol. 66, no. 3, pp. 666–681, Feb 2018.
- [43] G. Cheung, E. Magli, Y. Tanaka, and M. K. Ng, "Graph spectral image processing," *Proc. IEEE*, vol. 106, no. 5, pp. 907–930, May 2018.
- [44] C. Dinesh, G. Cheung, and I. V. Bajić, "Super-resolution of 3D color point clouds via fast graph total variation," in *Proc. IEEE ICASSP*, 2020, pp. 1983–1987.
- [45] C. Dinesh, G. Cheung, and I. V. Bajić, "3D point cloud color denoising using convex graph-signal smoothness priors," in *Proc. IEEE MMSP*, Sep. 2019, pp. 1–6.
- [46] C. Dinesh, G. Cheung, F. Wang, and I. V. Bajić, "Sampling of 3D point cloud via Gershgorin disc alignment," in *Proc. IEEE ICIP*, 2020, pp. 2736–2740.
- [47] W. Hu, X. Gao, G. Cheung, and Z. Guo, "Feature graph learning for 3D point cloud denoising," *IEEE Trans. Signal Process.*, vol. 68, pp. 2841–2856, 2020.
- [48] Z. Fu, W. Hu, and Z. Guo, "3D dynamic point cloud inpainting via temporal consistency on graphs," in *Proc. IEEE ICME*, 2020, pp. 1–6.
- [49] J. Qi, W. Hu, and Z. Guo, "Feature preserving and uniformity-controllable point cloud simplification on graph," in *Proc. IEEE ICME*, 2019, pp. 284–289.

- [50] J. Zeng, G. Cheung, M. Ng, J. Pang, and C. Yang, "3D point cloud denoising using graph laplacian regularization of a low dimensional manifold model," *IEEE Trans. Image Process.*, vol. 29, pp. 3474–3489, 2020.
- [51] C. Dinesh, G. Cheung, and I. V. Bajić, "Point cloud sampling via graph balancing and gershgorin disc alignment," *IEEE Trans. Pattern Anal. Mach. Intell.*, vol. 45, no. 1, pp. 868–886, 2023.
- [52] C. Dinesh, G. Cheung, and I. V. Bajić, "Point cloud video super-resolution via partial point coupling and graph smoothness," *IEEE Trans. Image Process.*, vol. 31, pp. 4117–4132, 2022.
- [53] Y. Schoenenberger, J. Paratte, and P. Vandergheynst, "Graph-based denoising for time-varying point clouds," in *IEEE 3DTV-Conference*, 2015, pp. 1–4.
- [54] F. R. Chung and F. C. Graham, *Spectral graph theory*, Number 92. American Mathematical Soc., 1997.
- [55] M. H. Kutner, C. J. Nachtsheim, J. Neter, and W. Li, *Applied Linear Statistical Models*, McGraw-Hill/Irwin, 5th edition, 2005.
- [56] L. E. Eberly, "Multiple linear regression," *Topics in Biostatistics*, pp. 165–187, 2007.